Available online at www.sciencedirect.com
ScienceDirect
Journal of Sound and Vibration 320 (2009) 707–725
JOURNAL OF SOUND AND VIBRATION
www.elsevier.com/locate/jsvi

An optimal stochastic control theory for distributed energy harvesting networks

J.T. Scruggs

Department of Civil and Environmental Engineering, Duke University, USA

Received 21 November 2007; received in revised form 26 August 2008; accepted 2 September 2008
Handling Editor: S. Bolton
Available online 16 October 2008

Abstract

A new approach, based on $\mathscr{H}_2$ optimal control theory, is presented for the design of feedback controllers for energy harvesting systems for maximal power generation. The theory applies to stochastically excited vibratory systems in broadband stationary response, and allows for harvested power to be explicitly optimized. It is applicable to both single-transducer systems as well as coupled networks of many transducers. The theory accounts for the influence of energy harvesting on the dynamics of the structure to which the transducers are attached. It also accounts for resistive and semiconductor dissipation in the power-electronic network interfacing the transducers with energy storage. Due to its predominance in the literature, a piezoelectric bimorph cantilever beam is used as the context for the theory, and simulation examples are used to illustrate various aspects of the optimal controllers.
© 2008 Elsevier Ltd. All rights reserved.

1. Introduction

There is a growing demand for engineering systems that are capable of operating in complete energy-autonomy for the duration of a decades-long service life. Examples include intelligent systems for biological implants, and wireless sensors for in situ structural health monitoring. This has given rise to significant activity over the last decade in energy scavenging technology to harvest power from ambient vibration. While many modes of transduction could be used for energy-scavenging, there is a growing consensus that piezoelectric approaches are often the most appropriate at the μW–mW scale, which is typical of these applications. There have been hundreds of studies on the transduction of electrical energy from a single piezoelectric transducer, bonded to a vibrating beam, in which its voltage is rectified through a full bridge rectifier, to which is connected a capacitor and rechargeable battery, or a resistive load. Sensitivity of the harvested power, due to changes in the transducer configuration, polarization, geometry, coupling coefficient, and dielectric constant as well as characteristics of the structure and external forcing have been investigated (see [1] and the many references therein).

Fig. 1 shows an example of the type of energy harvesting system to be considered here, in which a number of piezoelectric bimorph patches are bonded to a resonant flexible beam, and interfaced through an electronic

E-mail address: jeff.scruggs@duke.edu

0022-460X/$ - see front matter © 2008 Elsevier Ltd. All rights reserved.
doi:10.1016/j.jsv.2008.09.001

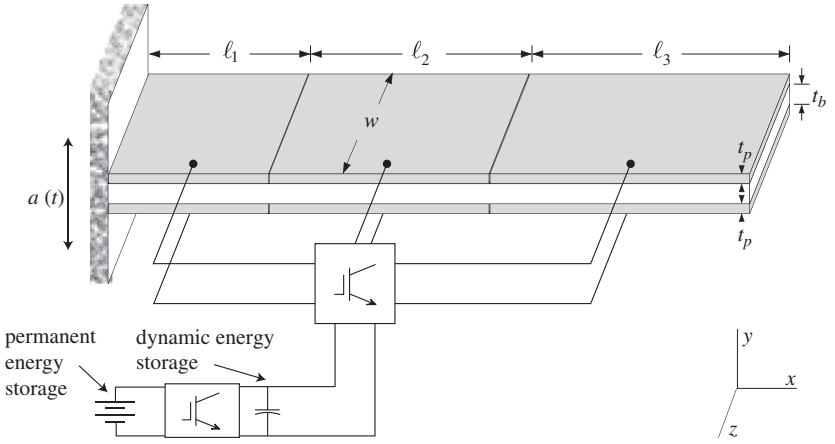

Fig. 1. Energy harvesting bimorph cantilever with distributed piezoelectric transducers (gray) bonded to a substrate (white).

network. Random vibration of the base mount causes the beam system to resonate in several of its flexible modes, and the resultant bending motion generates charge in the piezoelectric patches. Through proper power-electronic control, energy can be drawn from these patches and interfaced with energy storage, or recirculated back into the beam through another patch. The power electronics are controlled so as to impose a multi-input, multi-output control law on the structure, in which the goal is to maximize the harvested energy sent to storage.

Thus far, most studies regarding these types of energy harvesting systems have focused on single-transducer systems. Some of the first investigations into the design of power-electronic control systems for small-scale vibratory energy harvesting systems were reported in Refs. [2–4] as well as [5]. These studies examined the use of power-electronic control to achieve favorable supply recharge characteristics, by connection of a controllable DC–DC converter to the bridge rectifier. The external forcing was assumed to be harmonic, at the resonant frequency of the beam system, and the control design was based on the concept of impedance matching. More recently, systematic studies were conducted on the optimal matched impedance for harmonic excitation, and its sensitivity to other aspects of the system [6,7].

In 2003, it was suggested [8] that power transduction from piezoelectric devices might be improved through the use of a switchmode "H-bridge" drive, in exchange for the bridge rectifier used in previous designs. Recent years have seen a number of investigations [9–12] on the incorporation of power-electronic switches into the rectifier circuitry, resulting in several ad hoc active drive technologies. These studies proposed a number of heuristic switching rules and circuit topologies which allow much greater control of transduced energy, increasing power flow from the transducer significantly beyond that for simpler electronic systems.

Against this backdrop, the contributions of this paper are threefold. First, it is an investigation of the *optimal* way to control the currents in the power-electronic drive system to maximize the power delivered to storage, and illustrates that this problem may be framed in the context of $\mathscr{H}_2$ optimal control theory. This approach allows for dissipation in the electronics to be taken into account in the optimization.

The second contribution is that these concepts are framed in the context of broadband stochastic vibratory response. Most energy harvesting strategies proposed thus far have presumed harmonic excitation, or at least that the vibratory system has a high enough quality factor that this approximation is justifiable. The present analysis makes the opposite assumption, i.e., that the external disturbance is a white noise process. Thus, it provides an alternative approach which may be more appropriate for systems with multiple significant modes and wide excitation frequency band.

The third contribution is that the theory is applicable to *networks* of many transducers, as illustrated in Fig. 1. Methods for harvesting energy from arrays of dynamically coupled transducers in spatially distributed arrays has received recent attention [13,14], and the present analysis frames the management of power for these systems in a systematic control-theoretic context.

The notation is mostly standard. Bold lower-case notation will be used to refer to vectors, and bold upper-case for matrices. Expressions $\|\mathbf{q}\|_1$ and $\|\mathbf{q}\|_2$ refer to the "1-norm" and Euclidean norm of $\mathbf{q} \in \mathbb{R}^n$. Additionally, $\|\mathbf{q}\|_{\mathbf{Q}} = (\mathbf{q}^{\mathrm{T}}\mathbf{Q}\mathbf{q})^{1/2}$. Notation tr[**Q**] refers to the trace of matrix **Q**, and $\mathbf{Q} > 0$ implies that **Q** is positive-definite. Expression $\mathscr{E}[\mathbf{q}]$ refers to the expectation of stationary stochastic time-valued vector $\mathbf{q}(t)$, argmin[·] refers to the minimizing argument, and diag(a, b, c) refers to the diagonal matrix with the ordered scalar arguments along its diagonal. The notation $\hat{\mathbf{e}}_p$ refers to the unit vector in direction p. Notation $g \sim N(\mu, \sigma)$ implies that g is a Gaussian random variable with mean μ and standard deviation σ.

2. System model

2.1. Beam model

In Ref. [15], the electromechanical dynamics of a beam with multiple bimorph piezoelectric transducers were derived. Here, we present an overview of this model, while adopting many of simplifying assumptions made in Ref. [16].

Let $\rho(x, y, z, t)$ denote the density at location $\{x, y, z\}$ in the substrate–piezo composite. Let $\mathbf{S}(x, y, z, t) \in \mathbb{R}^6$ and $\mathbf{T}(x, y, z, t) \in \mathbb{R}^6$ denote the Voigt (i.e., vector) form of the strain and stress tensors, and let $\mathbf{E}(x, y, z, t) \in \mathbb{R}^3$ and $\mathbf{D}(x, y, z, t) \in \mathbb{R}^3$ denote the electric field and displacement vectors. We assume the linear constitutive relationship

$$\begin{bmatrix} \mathbf{T}(x,y,z,t) \\ \mathbf{D}(x,y,z,t) \end{bmatrix} = \begin{bmatrix} \mathbf{c}(x,y,z,t) & -\mathbf{e}^{\mathrm{T}}(x,y,z,t) \\ \mathbf{e}(x,y,z,t) & \boldsymbol{\varepsilon}(x,y,z,t) \end{bmatrix} \begin{bmatrix} \mathbf{S}(x,y,z,t) \\ \mathbf{E}(x,y,z,t) \end{bmatrix}, \tag{1}$$

where **c** is the modulus of elasticity at zero field, $\boldsymbol{\varepsilon}$ is the dielectric constant matrix at zero strain, and **e** is the coupling coefficient matrix. (Note that in the substrate material, **e** and $\boldsymbol{\varepsilon}$ are zero.)

To study the electromechanical dynamics in the context of the cantilever beam in Fig. 1, define $d(x, t)$ as the transverse deflection of the beam centroid, relative to the neutral axis. Then, the Bernoulli–Euler beam deformation assumption is made, i.e.,

$$\mathbf{S}(x, y, z, t) = y d''(x, t) \begin{bmatrix} \hat{\mathbf{e}}_x \\ \mathbf{0} \end{bmatrix}. \tag{2}$$

Deflection $d(x, t)$ is approximated in the usual way, by a finite summation of Galerkin functions, as

$$d(x, t) = \boldsymbol{\phi}^{\mathrm{T}}(x)\mathbf{r}(t), \tag{3}$$

where $\boldsymbol{\phi}(x) \in \mathbb{R}^N$ is a vector of x-valued Galerkin functions which satisfy boundary conditions and $\mathbf{r}(t) \in \mathbb{R}^N$ is the coordinate vector for the reduced system. We will use the convention of assigning these Galerkin functions to be mass-orthonormal, i.e.,

$$\int_V \boldsymbol{\phi}(x)\boldsymbol{\phi}^{\mathrm{T}}(x)\rho(x, y)\,\mathrm{d}V = \mathbf{I}. \tag{4}$$

This convention is not necessary for the ensuing analysis to work, but it does simplify the notation considerably.

To characterize the external mechanical loading, we assume the only excitation to be the base acceleration $a(t)$, which is assumed to be in the $\hat{\mathbf{e}}_y$ direction. In the coordinate system fixed at the base mount, this is equivalent to an external force

$$f(x, y, t) = \rho(x, y)a(t) \tag{5}$$

applied in the y direction.

Let the components of vectors $\mathbf{v}(t)$ and $\mathbf{i}(t)$ denote the voltages and currents for transducer patches $1, \ldots, n_p$. As shown in Fig. 1, the patches are assumed to be prismatic, with rectangular cross section, a common thickness t_p, and lengths $\{\ell_1, \ldots, \ell_{n_p}\}$. They are assumed to span the width w of the beam. The gaps between patches are assumed to be of negligible length, and are assumed to have no effect on beam stiffness. **E** is assumed to be constant inside each patch, zero in the substrate, and oriented in the $\hat{\mathbf{e}}_y$ direction

everywhere, i.e.,

$$\mathbf{E}(x,y,z,t) = \hat{\mathbf{e}}_y \psi(y) \boldsymbol{\zeta}^{\mathrm{T}}(x) \mathbf{v}(t), \tag{6}$$

where $\hat{\mathbf{e}}_y$ is the unit vector on the y direction, $\psi(y)$ is defined as

$$\psi(y) = \begin{cases} -1/t_p, & t_b/2 < y < t_b/2 + t_p, \\ 0, & -t_b/2 < y < t_b/2, \\ 1/t_p, & -t_b/2 - t_p < y < -t_b/2 \end{cases} \tag{7}$$

and $\boldsymbol{\zeta}(x)$ is a vector in which $\zeta_j(x)$ is the logical indicator function for patch j situated at location x along the beam.

With these assumptions, the differential equations for the reduced-order system are found through a standard Rayleigh–Ritz projection, giving differential equations for $\mathbf{r}$ and $\mathbf{v}$ as

$$\ddot{\mathbf{r}}(t) + \mathbf{K}\mathbf{r}(t) + \boldsymbol{\Theta}\mathbf{v}(t) = \boldsymbol{\Gamma} a(t), \tag{8}$$

$$\mathbf{C}_p \dot{\mathbf{v}}(t) - \boldsymbol{\Theta}^{\mathrm{T}} \dot{\mathbf{r}}(t) = \mathbf{i}(t), \tag{9}$$

where

$$\mathbf{K} = \int_V c_{xx}(x,y) y^2 \boldsymbol{\phi}''(x) \boldsymbol{\phi}''^{T}(x)\, \mathrm{d}V, \tag{10}$$

$$\boldsymbol{\Theta} = \int_V e_{yx}(x,y) y \psi(y) \boldsymbol{\phi}''(x) \boldsymbol{\zeta}^{\mathrm{T}}(x)\, \mathrm{d}V, \tag{11}$$

$$\mathbf{C}_p = \int_V \varepsilon_{yy}(x,y) \psi^2(y) \boldsymbol{\zeta}(x) \boldsymbol{\zeta}^{\mathrm{T}}(x)\, \mathrm{d}V, \tag{12}$$

$$\boldsymbol{\Gamma} = \int_V \boldsymbol{\phi}(x) \rho(x,y)\, \mathrm{d}V \tag{13}$$

and where c_{xx} is the $\{x,x\}$ component of $\mathbf{c}$, e_{yx} is the $\{y,x\}$ component of $\mathbf{e}$, and ε_{yy} is the $\{y,y\}$ component of $\boldsymbol{\varepsilon}$. Note that it has been assumed that these parameters, as well as the density ρ, are uniform in the z direction.

As pointed out in Ref. [16], it is crucial to include material damping in the beam model, in order for its predictions of transductive behavior to be reasonable. To reflect dissipation in the beam, Rayleigh damping will be added to differential equation (8) for $\mathbf{r}(t)$, i.e.,

$$\ddot{\mathbf{r}}(t) + \mathbf{C}\dot{\mathbf{r}}(t) + \mathbf{K}\mathbf{r}(t) + \boldsymbol{\Theta}\mathbf{v}(t) = \boldsymbol{\Gamma} a(t), \tag{14}$$

where $\mathbf{C}$ is assumed to have the form $\mathbf{C} = \alpha_M \mathbf{I} + \alpha_K \mathbf{K}$. Similarly, dielectric loss in the piezoelectric capacitances is introduced through a parallel resistance matrix $\mathbf{R}_p = \mathrm{diag}(R_{p1}, \ldots, R_{pn_p})$, modifying Eq. (9) to

$$\mathbf{C}_p \dot{\mathbf{v}}(t) + \mathbf{R}_p^{-1} \mathbf{v}(t) - \boldsymbol{\Theta}^{\mathrm{T}} \dot{\mathbf{r}}(t) = \mathbf{i}(t). \tag{15}$$

2.2. Power-electronic model

Because no two patches can occupy the same x coordinate, capacitance matrix $\mathbf{C}_p$ will in general be diagonal, with component $\{j,j\}$ equal to the capacitance of patch j. Consequently, we may represent the transducer network as in Fig. 2.

The drive current vector $\mathbf{i}(t)$ is controlled by operating the four switches, arranged in "H-bridge" configuration, which interface each transducer with the storage system voltage V_S. It will be assumed that V_S is large in comparison to $\mathbf{v}(t)$, which is true for sufficiently low excitation levels, and can always be ensured through proper design and power management of the energy storage subsystem. (Removal of this assumption, which results in a somewhat more complicated analysis, was recently considered in Ref. [17].) It will also be

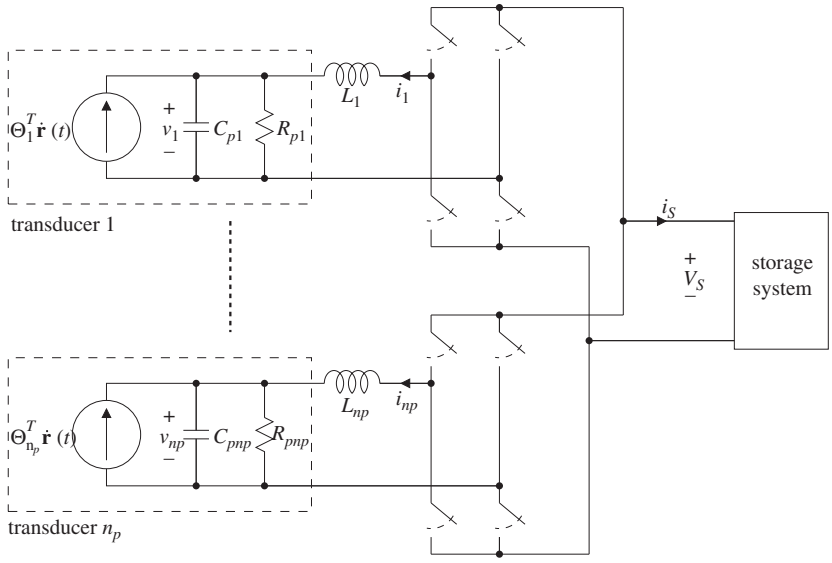

Fig. 2. Drive circuitry for distributed energy harvesting system.

assumed that the input impedance of the storage subsystem may be neglected, and that voltage V_S remains constant, independently of the current i_S. This assumption is justified for sufficiently low power levels. A relaxation of these assumptions, which greatly complicates the analysis, remains an item for future work.

Through appropriate operation of the switches in the H-bridge for each transducer, the voltage across each inductor can be made positive or negative (this comes from the assumption that V_S is large). As such, these switches can be used to raise and lower the currents $\mathbf{i}$. High-bandwidth current tracking for power-electronic drives, using either pulse width modulation or hysteretic switching paradigms, is a well-understood technology (see, for example, Ref. [18]). To simplify the analysis here, it will here be assumed that such a tracking control system can be used to instantaneously produce a desired current vector for $\mathbf{i}(t)$. There are many theoretical and practical considerations which must be taken into account in the design of the power-electronic hardware and current tracking controller, such that this approximation is justified [19,20]. However, it is beyond the scope of the present study to delve into these details.

Under these assumptions, the net power flow into the piezoelectric patches is

$$P_p(t) = \mathbf{i}^{\mathrm{T}}(t)\mathbf{v}(t). \tag{16}$$

The power flow to storage from the network is

$$P_S(t) = i_S(t)V_S(t). \tag{17}$$

If the drive system were 100% efficient, then $P_S(t) = -P_p(t)$. However, in general there are resistive and semiconductor losses in the drive, which will be denoted as $P_d(t)$. We will assume that this power flow may be approximated as

$$P_d(t) = \mathbf{i}^{\mathrm{T}}(t)\mathbf{R}\mathbf{i}(t) + \sum_{j=1}^{n_p} |i_j(t)|V_{sw}. \tag{18}$$

The first term above reflects resistive (i.e., "i^2R") losses in the drive. The terms in the summation reflect semiconductor dissipation in the drive switches, which are approximately the product of the activation voltage of the switch (V_{sw}) and the current magnitude.

Although the above approximation can be used to capture some of the primary sources of dissipation in the drive system, it is acknowledged that it is an *approximation* and does not account for all losses. For example, it does not reflect switch transition losses, core losses in the inductor, or the power required for the gate drives. For an application where these losses dominate, the theory proposed here will require extension.

2.3. Example parameters

In this paper we will routinely resort to examples to illustrate the analytical concepts. Table 1 shows the physical constants used in all these examples, which were adapted from the example in Ref. [16], in which the piezoelectric material was lead zirconium titanate (PZT). The remaining unspecified parameters (such as n_p, $\{\ell_1,\ldots,\ell_{n_p}\}$, R_j, etc.) will vary from one specific example to the next.

The Galerkin functions to be used in the approximate analysis will be the first seven mode shapes of a uniform cantilever Euler–Bernoulli beam, i.e.,

$$\phi_j(x) \propto [\sin(\beta_j\ell) - \sinh(\beta_j\ell)][\sinh(\beta_j x) - \sin(\beta_j x)] + [\cos(\beta_j\ell) + \cosh(\beta_j\ell)][\cosh(\beta_j x) - \cos(\beta_j x)], \tag{19}$$

where the β_j values satisfy

$$\cos(\beta_j\ell)\cosh(\beta_j\ell) = -1. \tag{20}$$

With the piezoelectrics short-circuited (i.e., with $\mathbf{v} = \mathbf{0}$), the beam model reduces to the standard Bernoulli–Euler beam, and the above mode shapes become exact. Rayleigh damping parameters were assigned such that for this scenario the first seven modes have natural frequencies and damping ratios given by Table 2. For modeling purposes, $\zeta_j = \infty$ was effectively assumed for $j > 7$.

2.4. Linear state-space representation

With the above modeling assumptions for the electromechanical system, we may consider the dynamic system at hand to be characterized by the augmented state vector

$$\mathbf{x} = \begin{bmatrix} \mathbf{K}^{1/2} & \mathbf{0} & \mathbf{0} \\ \mathbf{0} & \mathbf{I} & \mathbf{0} \\ \mathbf{0} & \mathbf{0} & \mathbf{C}_p^{1/2} \end{bmatrix} \begin{bmatrix} \mathbf{r} \\ \dot{\mathbf{r}} \\ \mathbf{v} \end{bmatrix}. \tag{21}$$

Table 1
Example parameters for beam with three bimorph transducers

ε_{yy}	$1800\varepsilon_0$
e_{yx}	$-11.3\,\mathrm{Pa/V}$
c_{xx} (piezo)	63 GPa
(substrate)	2.5 GPa
ρ (piezo)	$7700\,\mathrm{kg/m^3}$
(substrate)	$2150\,\mathrm{kg/m^3}$
ℓ	100 mm
t_b	0.25 mm
t_p	0.25 mm
w	25 mm
$C_{pj}R_{pj}$	2 s

Table 2
Natural frequencies and damping ratios for example beam

Mode	ω_i (rad/s)	$\zeta_i \times 100$
1	241	1.0
2	1510	4.4
3	4220	12
4	8270	24
5	13,700	39
6	20,400	58
7	28,500	82

In this notation, the total electromechanical energy in the beam is $E(t) = \frac{1}{2}\mathbf{x}^{\mathrm{T}}(t)\mathbf{x}(t)$, and the linear state-space system dynamics are described by

$$\dot{\mathbf{x}}(t) = \mathbf{A}\mathbf{x}(t) + \mathbf{B}_{\mathbf{i}}\mathbf{i}(t) + \mathbf{B}_a a(t), \tag{22}$$

$$\mathbf{v}(t) = \mathbf{B}_{\mathbf{i}}^{\mathrm{T}}\mathbf{x}(t), \tag{23}$$

where

$$\mathbf{A} = \begin{bmatrix} \mathbf{0} & \mathbf{K}^{1/2} & \mathbf{0} \\ -\mathbf{K}^{1/2} & -\mathbf{C} & -\boldsymbol{\Theta}\mathbf{C}_p^{-1/2} \\ \mathbf{0} & \mathbf{C}_p^{-1/2}\boldsymbol{\Theta}^{\mathrm{T}} & -\mathbf{C}_p^{-1/2}\mathbf{R}_p^{-1}\mathbf{C}_p^{-1/2} \end{bmatrix}, \tag{24}$$

$$\mathbf{B}_a = \begin{bmatrix} \mathbf{0} \\ \boldsymbol{\Gamma} \\ \mathbf{0} \end{bmatrix}, \quad \mathbf{B}_{\mathbf{i}} = \begin{bmatrix} \mathbf{0} \\ \mathbf{0} \\ \mathbf{C}_p^{-1/2} \end{bmatrix}. \tag{25}$$

Note that in the system realization above, matrix $\mathbf{B}_{\mathbf{i}}$ exhibits reciprocity as both an input matrix in Eq. (22) and a collocated output matrix in Eq. (23).

In this analysis $a(t)$ is modeled as a Gaussian white noise process, with spectral intensity of Φ_a. However, it is straightforward to extend the ideas presented here to the case in which $a(t)$ is assumed to have nontrivial spectral characteristics, by modeling $a(t)$ as a linear stochastic dynamic process, and augmenting the states of this process to the state vector $\mathbf{x}$.

2.5. Preliminary observations regarding power flow

Let $P_A(t)$ be the mechanical power flow from disturbance $a(t)$, to the system. Then for $a(t)$ modeled as white noise, we summarize some useful observations from general stochastic vibration theory.

Lemma 1. *Let* $\mathbf{i}$ *be related to the system response by any stabilizing, causal feedback function, and assume that all modes above the first N have infinite damping. Then in stationary response, the average power absorbed by the first N modes is equal to*

$$\bar{P}_A^N = \tfrac{1}{2}\Phi_a \mathbf{B}_a^{\mathrm{T}}\mathbf{B}_a. \tag{26}$$

Proof. From Eqs. (22) and (23), we have that

$$\dot{E}(t) = \tfrac{1}{2}[\mathbf{x}^{\mathrm{T}}(t)\dot{\mathbf{x}}(t) + \dot{\mathbf{x}}^{\mathrm{T}}(t)\mathbf{x}(t)]. \tag{27}$$

But inspection of Eq. (24) implies that the dissipation associated with state $\mathbf{x}$ is

$$P_{\mathbf{x}}(t) = -\mathbf{x}(t)^{\mathrm{T}}\mathbf{A}\mathbf{x}(t) \tag{28}$$

and the power injected into the state-space model by the drive is

$$P_p(t) = \mathbf{x}^{\mathrm{T}}(t)\mathbf{B}_{\mathbf{i}}\mathbf{i}(t). \tag{29}$$

Thus, from energy conservation, we have that the power driven into the state-space by acceleration $a(t)$ is $\dot{E} - P_p + P_{\mathbf{x}}$, i.e.,

$$P_A^N(t) = \mathbf{x}^{\mathrm{T}}(t)\mathbf{B}_a a(t). \tag{30}$$

It is a standard result of stochastic system theory [21] that if $\mathbf{x} \to \mathbf{i}$ is a causal mapping, the expectation of the above is Eq. (26). □

One may ask why it is that we should distinguish $\bar{P}_A^N$ from $\bar{P}_A$, i.e., if the only modes excluded from the computation of $\bar{P}_A^N$ have infinite damping, then their response amplitudes are infinitesimal, suggesting that

$\bar{P}_A^N = \bar{P}_A$. However, this is not true. Consider, for example, the classical result that a single dof oscillator, subjected to a white noise base acceleration, dissipates the same amount of average power irrespective of its damping [22]. This is evident in the fact that the system damping does not figure into the computation of $\bar{P}_A^N$. Even though the higher modes are infinitely damped and have negligible dynamics, they *do* still dissipate a finite amount of energy for the modeling assumptions made here.

Lemma 2. *Let m be the total mass of the beam. Then*

$$\bar{P}_A = \lim_{N\to\infty} \bar{P}_A^N \tag{31}$$

$$= \frac{1}{2} m \Phi_a. \tag{32}$$

Proof. Let $u(x)$ be the Heaviside step function, and let $\mathbf{m}$ be its components in the $\mathscr{L}_2$ Hilbert space spanned by $\boldsymbol{\phi}$ for $N \to \infty$, i.e., $\|u - \boldsymbol{\phi}^{\mathrm{T}}\mathbf{m}\|_{\mathscr{L}_2} = 0$. Then from Eq. (13), for $N \to \infty$,

$$\boldsymbol{\Gamma} = \int_V \rho(x,y)\boldsymbol{\phi}(x)\,\mathrm{d}V = \left[\int_V \rho(x,y)\boldsymbol{\phi}(x)\boldsymbol{\phi}^{\mathrm{T}}(x)\,\mathrm{d}V\right]\mathbf{m} = \mathbf{m}. \tag{33}$$

Thus, under the $\mathscr{L}_2$ measure, $\boldsymbol{\Gamma} = \mathbf{m}$, and $\boldsymbol{\phi}^{\mathrm{T}}(x)\boldsymbol{\Gamma} = u(x)$. From Eq. (25), $\mathbf{B}_a^{\mathrm{T}}\mathbf{B}_a = \boldsymbol{\Gamma}^{\mathrm{T}}\boldsymbol{\Gamma}$, and therefore

$$\begin{aligned}\boldsymbol{\Gamma}^{\mathrm{T}}\boldsymbol{\Gamma} &= \boldsymbol{\Gamma}^{\mathrm{T}}\left[\int_V \rho(x,y)\boldsymbol{\phi}(x)\boldsymbol{\phi}^{\mathrm{T}}(x)\,\mathrm{d}V\right]\boldsymbol{\Gamma}\\ &= \int_V \rho(x,y)(\boldsymbol{\phi}^{\mathrm{T}}(x)\boldsymbol{\Gamma})^2\,\mathrm{d}V\\ &= \int_V \rho(x,y)\,\mathrm{d}V = m.\end{aligned} \tag{34}$$

By Lemma 1, we have Eq. (32). □

From Eqs. (16), (17), and (18), the goal of the energy harvesting control system is to control $\mathbf{i}(t)$ so as to maximize the expectation of $P_S(t)$, i.e.,

$$\begin{aligned}\bar{P}_S &= \mathscr{E}[P_S]\\ &= -\mathscr{E}[\mathbf{i}^{\mathrm{T}}(t)\mathbf{v}(t) + \mathbf{i}^{\mathrm{T}}(t)\mathbf{R}\mathbf{i}(t) + V_{sw}\|\mathbf{i}(t)\|_1].\end{aligned} \tag{35}$$

The conversion efficiency η is defined as

$$\eta = \frac{\bar{P}_S}{\bar{P}_A}. \tag{36}$$

Note that from Lemma 1, $\bar{P}_A$ is independent of $\mathbf{i}$. Also, while $\bar{P}_A$ does depend on the mass distribution of the patches along the beam, it is independent of where these patches are partitioned, or how many partitions there are. It follows from this observation that for white noise excitation, the energy harvesting controller which maximizes $\bar{P}_S$ is the same as the controller which maximizes η. This is an interesting consequence of the assumption that $a(t)$ is perfect white noise. Under different assumptions, maximization of efficiency is not necessarily the same as maximization of $\bar{P}_S$, because some controllers will result in higher $\bar{P}_A$ than others.

3. Optimal energy harvesting in the presence of resistive drive losses

In this section we consider the case where $V_{sw} = 0$, i.e., the case in which the semiconductor switches are presumed to be 100% efficient. Note that this assumption still allows for a nonzero drive resistance matrix $\mathbf{R}$. In fact, it will be assumed in the sequel that the drive resistance matrix is positive-definite, i.e., $\mathbf{R} > 0$. With $V_{sw} = 0$, we have that

$$\bar{P}_S = -\mathscr{E}[\mathbf{i}^{\mathrm{T}}(t)\mathbf{v}(t) + \mathbf{i}^{\mathrm{T}}(t)\mathbf{R}\mathbf{i}(t)]. \tag{37}$$

3.1. State feedback

We now show that the optimal causal control of current vector $\mathbf{i}$ constitutes a linear feedback function of the system state $\mathbf{x}$, and that the optimal feedback relationship can be found from standard $\mathscr{H}_2$ optimal control theory, through the solution to an associated Riccati equation.

Theorem 1. *Let* $\mathbf{A}$ *be asymptotically stable, and assume* $V_{sw}=0$. *Then over the space of all causal, continuous feedback functions of the dynamic system response, the optimal energy-harvesting current is characterized by the linear state feedback relationship*

$$\mathbf{i}(t)=\mathbf{F}\mathbf{x}(t), \tag{38}$$

where

$$\mathbf{F}=-\mathbf{R}^{-1}\mathbf{B}_{\mathbf{i}}^{\mathrm{T}}\mathbf{P} \tag{39}$$

and $\mathbf{P}>0$ *is the unique solution to the associated Riccati equation*

$$\mathbf{0}=-\tfrac{1}{2}[\mathbf{A}+\mathbf{A}^{\mathrm{T}}]+\mathbf{A}^{\mathrm{T}}\mathbf{P}+\mathbf{P}\mathbf{A}-\mathbf{P}\mathbf{B}_{\mathbf{i}}\mathbf{R}^{-1}\mathbf{B}_{\mathbf{i}}^{\mathrm{T}}\mathbf{P}. \tag{40}$$

The optimal harvested power is

$$\bar{P}_S=\Phi_a\mathbf{B}_a^{\mathrm{T}}[\tfrac{1}{2}\mathbf{I}-\mathbf{P}]\mathbf{B}_a>0. \tag{41}$$

Proof. The total power dissipated in the first N modes of the beam, the piezoelectric impedance, and power-electronic drive is

$$P_{\mathrm{diss}}=-\mathbf{x}^{\mathrm{T}}\mathbf{A}\mathbf{x}+\mathbf{i}^{\mathrm{T}}\mathbf{R}\mathbf{i}. \tag{42}$$

From Lemma 1, we have the energy conservation relationship

$$\begin{aligned}-\bar{P}_S&=\mathscr{E}[P_{\mathrm{diss}}]-\bar{P}_A^N\\&=\mathscr{E}[\tfrac{1}{2}\mathbf{x}^{\mathrm{T}}[-\mathbf{A}-\mathbf{A}^{\mathrm{T}}]\mathbf{x}+\mathbf{i}^{\mathrm{T}}\mathbf{R}\mathbf{i}]-\tfrac{1}{2}\Phi_a\mathbf{B}_a^{\mathrm{T}}\mathbf{B}_a.\end{aligned} \tag{43}$$

Thus, the optimal energy harvesting control problem can be reframed as the minimization of the expectation on the right-hand side of the equation above. Because $\mathbf{A}$ is asymptotically stable and $\mathbf{A}+\mathbf{A}^{\mathrm{T}}\leqslant 0$, it immediately follows as a standard result form $\mathscr{H}_2$ optimal control [23] that the feedback law to minimize this function exists, is linear, is characterized by Eqs. (38), (39) and (40), that

$$\mathscr{E}[P_{\mathrm{diss}}]=\Phi_a\mathbf{B}_a^{\mathrm{T}}\mathbf{P}\mathbf{B}_a \tag{44}$$

holds for the closed-loop system, and that $\mathbf{P}>0$. The last inequality in Eq. (41) is due to the fact that $\mathbf{i}=\mathbf{0}$ is in the domain over which the control was optimized, and yields $\bar{P}_S=0$. □

It is interesting to note that if optimal controller (38) is implemented, then the optimal efficiency is

$$\eta_{\mathrm{opt}}=\frac{\mathbf{B}_a^{\mathrm{T}}\mathbf{B}_a-2\mathbf{B}_a^{\mathrm{T}}\mathbf{P}\mathbf{B}_a}{m}. \tag{45}$$

This constitutes the upper bound on efficiency, resulting from limitations of the hardware. For finite $\mathbf{R}$, it is physically realizable if $\mathbf{x}$ can be measured with certainty at every time. However, this is usually not reasonable, and consequently the controller in Theorem 1 is generally impractical. Later, this will be rectified through the use of an observer, resulting in only the transducer voltages being necessary for feedback, thus effectively eliminating the need for sensors altogether. However, Theorem 1 does provide very useful insights into the physical limitations of energy harvesting systems, and can be used to explore the way hardware parameters affect these limitations.

The results from Theorem 1 raise interesting questions about optimal energy harvesting control, for the case where the drive is very efficient, i.e., $\mathbf{R}\to\mathbf{0}$. This case has a well-known control-theoretic interpretation, called "cheap control" [24,25], which is concerned with the limiting values for $\mathbf{P}$ and $\mathbf{F}$ for $\mathbf{R}=r\mathbf{I}$, with $r\to 0$.

Substitution of the equations for cheap control into the system at hand gives

$$\lim_{r\to 0}\mathbf{P} = \mathbf{B}_{\mathbf{i}\perp}\mathbf{P}_0\mathbf{B}_{\mathbf{i}\perp}^{\mathrm{T}}, \tag{46}$$

$$\lim_{r\to 0}\sqrt{r}\mathbf{F} = [[\mathbf{0} \quad -\mathbf{R}_p^{1/2}\boldsymbol{\Theta}^{\mathrm{T}}]\mathbf{P}_0 \quad -\mathbf{R}_p^{-1/2}\mathbf{C}_p^{-1/2}], \tag{47}$$

where $\mathbf{B}_{\mathbf{i}\perp} = [\mathbf{I} \;\; \mathbf{0}]^{\mathrm{T}}$ and $\mathbf{P}_0$ is the solution to the Riccati equation

$$\mathbf{0} = \begin{bmatrix}\mathbf{0} & \mathbf{0}\\ \mathbf{0} & \mathbf{C}\end{bmatrix} + \begin{bmatrix}\mathbf{0} & -\mathbf{K}^{-1/2}\\ \mathbf{K}^{1/2} & -\mathbf{C}\end{bmatrix}\mathbf{P}_0 + \mathbf{P}_0\begin{bmatrix}\mathbf{0} & \mathbf{K}^{1/2}\\ -\mathbf{K}^{-1/2} & -\mathbf{C}\end{bmatrix} - \mathbf{P}_0\begin{bmatrix}\mathbf{0} & \mathbf{0}\\ \mathbf{0} & \boldsymbol{\Theta}\mathbf{R}_p\boldsymbol{\Theta}^{\mathrm{T}}\end{bmatrix}\mathbf{P}_0. \tag{48}$$

Thus, we have that the maximum physically attainable efficiency for a given beam and transducer configuration, irrespective of the drive hardware used, is

$$\lim_{r\to 0}\eta_{\mathrm{opt}} = \frac{1}{m}\mathbf{B}_a^{\mathrm{T}}\left[\mathbf{I} - 2\mathbf{B}_{\mathbf{i}\perp}\mathbf{P}_0\mathbf{B}_{\mathbf{i}\perp}^{\mathrm{T}}\right]\mathbf{B}_a. \tag{49}$$

However, asymptotic achievement of this efficiency results in $\mathbf{F}\to\infty$, and is therefore not reachable, even if a lossless drive existed, and full-state feedback were practical.

Theorem 1 can be used to explore the way that different system parameters affect the physical limit on energy harvesting performance, which can be used to optimize system hardware. Here, we illustrate this through the optimization of ℓ_1 and ℓ_2 (with the understanding that $\ell_3 = \ell - \ell_1 - \ell_2$), for optimal total power transduction.

The top left plot in Fig. 3 shows η_{opt} over the domain of allowable $\{\ell_1/\ell, \ell_2/\ell\}$ values, under the assumption of a lossless drive. For this assumption, the "cheap control" approach is used to calculate η_{opt} as in Eq. (49).

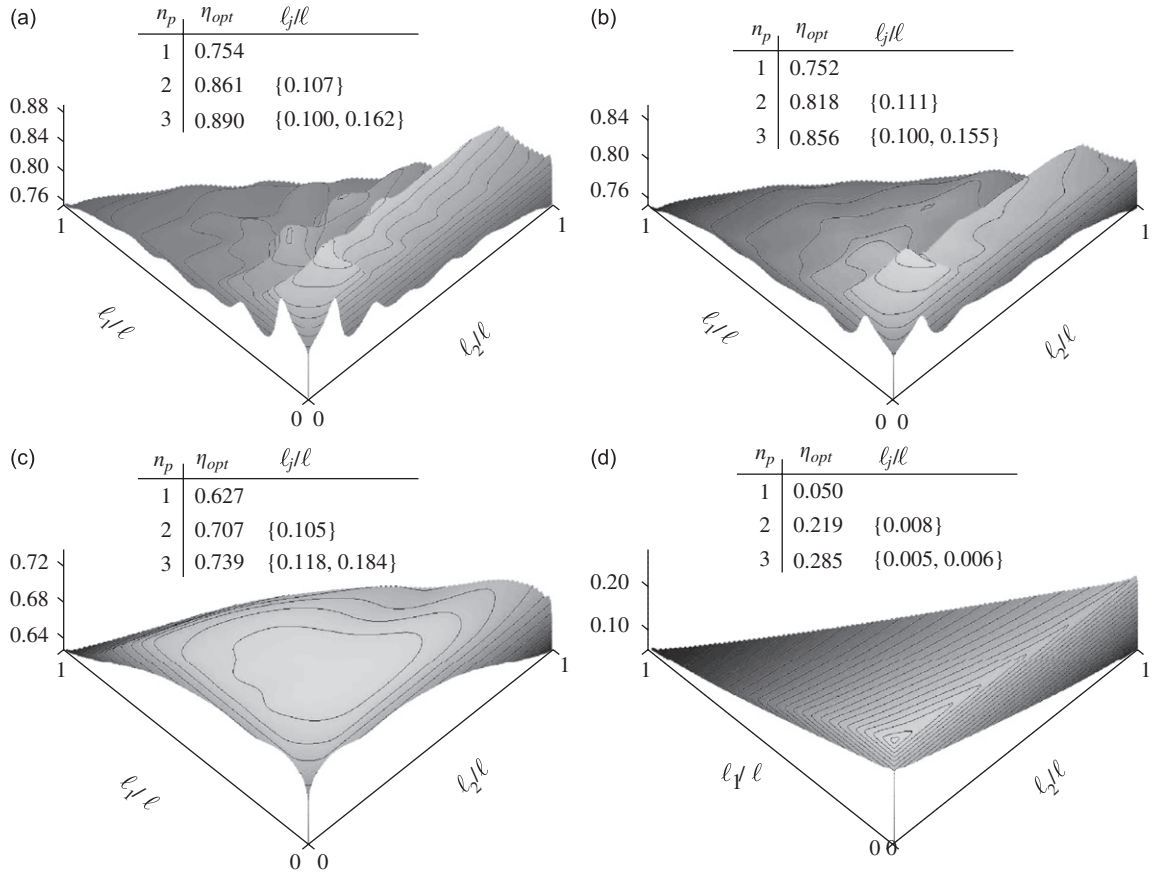

Fig. 3. Dependence of η_{opt} on $\{\ell_1, \ell_2\}$, with $\ell_3 = \ell - \ell_1 - \ell_2$, for R_j values of 0 Ω (a), 0.1 Ω (b), 100 Ω (c), and 100 kΩ (d).

This plot is useful because it allows us to consider the maximum physically attainable efficiency independently of the drive hardware. Above the plot, maximum efficiencies for one, two, and three patches are listed. The optimal three-patch efficiency is attained with $\{\ell_1/\ell, \ell_2/\ell\} = \{.100, .162\}$. The value of the maximum on the boundary of the domain is the optimal efficiency with two patches, while the single-patch efficiencies are those at the corners of the domain. Percentages of improvement for two and three patches, over one continuous patch, are 13% and 18%, respectively.

It is interesting to note that the efficiency of the drive circuitry has a strong impact not only on the amount of power which can be harvested, but also on the optimal patch locations along the beam. In addition to the lossless case, Fig. 3 shows contour plots for $R_j = 0.1\,\Omega$, $10\,\Omega$, and $100\,\Omega$. As expected, as the drive impedance increases, the ability of the system to harvest energy decreases. However, the important point here is that the optimal locations of the patches change as well. It is also interesting to note that the increasing drive resistance has the effect of "smoothing out" the dependency of efficiency on the patch lengths.

3.2. Transducer voltage feedback

We now consider the formulation of a dynamic feedback controller that determines $\mathbf{i}$ from $\mathbf{v}$. Such a system requires no structural sensors, which is highly appealing in an application in which energy efficiency is the primary concern. We now state, without proof, a standard lemma which provides the framework for control design.

Lemma 3. *Let* $\mathbf{K} : \mathbf{v} \to \mathbf{i}$ *be any causal, continuous (possibly nonlinear) feedback law, and assume* $\mathbf{R} > 0$. *Then the absorbed power in stationary response is*

$$\bar{P}_S = \Phi_a \mathbf{B}_a^{\mathrm{T}} [\tfrac{1}{2}\mathbf{I} - \mathbf{P}]\mathbf{B}_a - \mathscr{E}\|\mathbf{i} - \mathbf{F}\mathbf{x}\|_{\mathbf{R}}^2, \tag{50}$$

where $\mathbf{F}$ *is as in Eq.* (39).

Proof. See, for example, Ref. [21]. □

We will only consider linear dynamic controllers of the form

$$\mathbf{i}(s) = \mathbf{K}(s)\mathbf{v}(s). \tag{51}$$

From Eq. (50), the underlying goal for the design of $\mathbf{K}(s)$ is to minimize the quantity $\mathscr{E}\|\mathbf{i} - \mathbf{F}\mathbf{x}\|_{\mathbf{R}}^2$. However, this minimization is subject to limitations of the control and sensor hardware, such as bandwidth limitations, gain limitations, pole placement limitations, noise corruption, and complexity. The degree to which these diverse constraints restrict $\mathbf{K}(s)$ will ultimately vary from one application to another, as dictated by control, sensor, and power-electronic hardware, and will significantly modify the way in which the design should proceed.

In this paper, we consider only the very simplest case, in which $\mathbf{v}$ is measured in the presence of broadband noise, resulting in the optimal $\mathbf{K}(s)$ as a Kalman filter which operates on feedback law (38). However, it should be noted that this scenario was chosen simply for brevity. For the case in which one of the other aforementioned control limitations dominates, or in which several limitations should be enforced simultaneously, $\mathbf{K}(s)$ can still be designed systematically [26]. However, the exposition associated with these design methods was deemed beyond the scope of this paper.

Theorem 2. *Let the measurement noise of the transducer voltages to be a white noise process* $\mathbf{n}(t) \in \mathbb{R}^{n_p}$ *with spectral intensity* $\mathbf{\Phi}_n > 0$. *Then the optimal energy harvesting controller is*

$$\mathbf{K}(s) = -\mathbf{F}[s\mathbf{I} - \mathbf{A} - \mathbf{B}_{\mathbf{i}}\mathbf{F} - \mathbf{L}\mathbf{B}_{\mathbf{i}}^{\mathrm{T}}]^{-1}\mathbf{L}, \tag{52}$$

where

$$\mathbf{L} = -\mathbf{W}\mathbf{B}_{\mathbf{i}}\mathbf{\Phi}_n^{-1} \tag{53}$$

and $\mathbf{W} > 0$ *is the unique solution to Riccati equation*

$$\mathbf{0} = \mathbf{B}_a \Phi_a \mathbf{B}_a^{\mathrm{T}} + \mathbf{A}\mathbf{W} + \mathbf{W}\mathbf{A}^{\mathrm{T}} - \mathbf{W}\mathbf{B}_{\mathbf{i}}\mathbf{\Phi}_n^{-1}\mathbf{B}_{\mathbf{i}}^{\mathrm{T}}\mathbf{W}. \tag{54}$$

The optimal absorbed power is then

$$\bar{P}_S = \Phi_a \mathbf{B}_a^{\mathrm{T}}[\tfrac{1}{2}\mathbf{I} - \mathbf{P}]\mathbf{B}_a - \mathrm{tr}[\mathbf{W}\mathbf{F}^{\mathrm{T}}\mathbf{R}\mathbf{F}] \tag{55}$$

$$= \mathrm{tr}[\mathbf{\Phi}_n \mathbf{L}^{\mathrm{T}}[\tfrac{1}{2}\mathbf{I} - \mathbf{P}]\mathbf{L}] \tag{56}$$

$$> 0. \tag{57}$$

Proof. For the performance functional in Lemma 3, Eqs. (52), (53), (54) and (55) are standard results [23,21]. It is straightforward to show that Eq. (55) is equivalent to

$$\bar{P}_S = \Phi_a \mathbf{B}_a^{\mathrm{T}}[\tfrac{1}{2}\mathbf{I} - \mathbf{P}]\mathbf{B}_a - \Phi_a \mathbf{B}_a^{\mathrm{T}}\mathbf{X}\mathbf{B}_a + \mathrm{tr}[\mathbf{\Phi}_n \mathbf{L}^{\mathrm{T}}\mathbf{X}\mathbf{L}], \tag{58}$$

where $\mathbf{X} > 0$ is the solution to

$$\mathbf{0} = \mathbf{A}^{\mathrm{T}}\mathbf{X} + \mathbf{X}\mathbf{A} + \mathbf{F}^{\mathrm{T}}\mathbf{R}\mathbf{F}. \tag{59}$$

But the solution to the above is $\mathbf{X} = -\mathbf{P} + \frac{1}{2}\mathbf{I}$, thus giving Eq. (56). Inequality (57) is due to the fact that $\mathbf{K} = \mathbf{0}$ is in the optimization domain, and yields $\bar{P}_S = 0$. □

One interesting issue brought to light by Theorem 2 is the way in which the ability to measure $\mathbf{v}$ precisely affects the optimal amount of power that can be harvested. To illustrate this, we return again to the example from Section 2.3, with ℓ_1/ℓ and ℓ_2/ℓ equal to 0.118 and 0.184; the optimal parameters in Fig. 3 for $R_j = 100\,\Omega$. For this system, Fig. 4 shows the way in which $\mathbf{\Phi}_n = \Phi_n \mathbf{I}$ affects $\bar{P}_S$ for increasing Φ_n. Such plots as this can be used to ascertain the accuracy of feedback measurements which is required for a given application.

Even with perfect measurements for $\mathbf{v}$, the above control synthesis is useful because by increasing Φ_n, the closed-loop control bandwidth can be indirectly reduced. Furthermore, in this case a simple Lyapunov

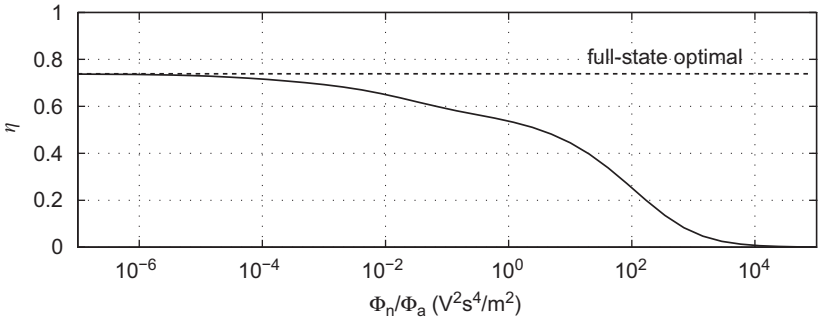

Fig. 4. Dependence of optimal conversion efficiency on Φ_n, for $R_j = 100\,\Omega$.

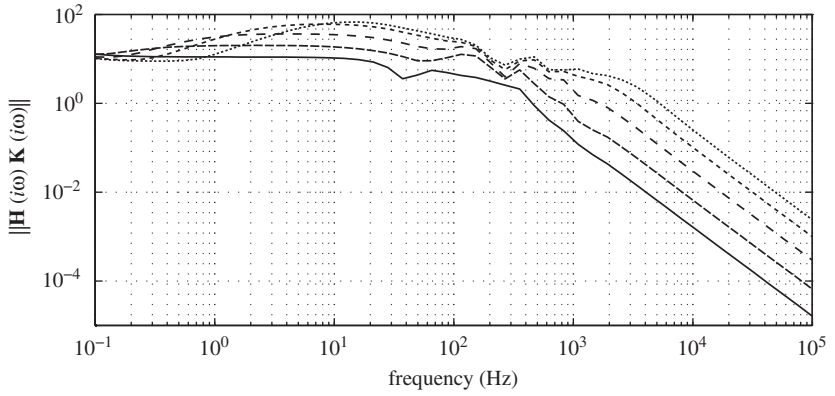

Fig. 5. System loop gain for $R_j = 100\,\Omega$, with various Φ_n/Φ_a values (in $\mathrm{V}^2\,\mathrm{s}^4/\mathrm{m}^2$): ····· 10^{-6}, - - - - - - - - 10^{-5}, – – – – 10^{-4}, ———— 10^{-3}, ———— 10^{-2}.

argument can be used to show that the value of η obtained by this procedure is bounded from below by the values given in Theorem 2 for the case where the measurement noise actually exists. Consequently, this procedure, while sub-optimal, still guarantees a certain threshold of energy conversion efficiency.

Fig. 5 shows this dependency, for the $R_j = 100\,\Omega$ case. The figure shows the maximum singular value of the feedback system loop gain $\mathbf{H}(s)\mathbf{K}(s)$, where $\mathbf{H}(s)$ is the transfer function from $\mathbf{i}$ to $\mathbf{v}$. In order for the closed-loop controller dynamics to have a bandwidth below some ω_0, the maximum singular value of the loop gain should have a crossover frequency at or below ω_0. So, for example, if a closed-loop bandwidth of 1 kHz is desired, then $10^{-4} < \Phi_n/\Phi_a < 10^{-3}\,\mathrm{V^2\,s^4/m^2}$ is reasonable. This would in turn result in a lower bound for η between 0.66 and 0.70, according to Fig. 4. Finally, we note that as $\Phi_n \to 0$, the control bandwidth becomes large, and the controller approaches the performance of full-state controller (38).

4. Extension to systems with semiconductor drive losses

We now return to the general expression for $\bar{P}_S$, Eq. (35), which includes both resistive and semiconductor dissipation terms. In this section, we extend the results of the last section to accommodate $V_{sw} \neq 0$. We note, however, that the methods presented here are sub-optimal, because only linear controllers will be considered. It is freely acknowledged that in the presence of semiconductor switching losses, there may be nonlinear controllers which outperform the ones presented here. However, the methods presented here *do* still give the optimal linear control.

In general we have that

$$\bar{P}_S = -\mathscr{E}[\mathbf{i}^{\mathrm{T}}\mathbf{v} + \mathbf{i}^{\mathrm{T}}\mathbf{R}\mathbf{i}] - \mathscr{E}[V_{sw}\|\mathbf{i}\|_1]. \tag{60}$$

The first expectation on the right-hand side is the value of $\bar{P}_S$ in the absence of semiconductor dissipation. The second term is the depreciation in this absorbed power due to semiconductor dissipation. We now define the *equivalent switch resistance* $\mathbf{R}_{sw} = \mathrm{diag}\{\ldots, R_{swj}, \ldots\}$ such that in stationary response

$$R_{swj}\mathscr{E}[i_j^2] = \mathscr{E}[V_{sw}|i_j|]. \tag{61}$$

Thus defined, we have that

$$\bar{P}_S = -\mathscr{E}[\mathbf{i}^{\mathrm{T}}\mathbf{v} + \mathbf{i}^{\mathrm{T}}(\mathbf{R} + \mathbf{R}_{sw})\mathbf{i}]. \tag{62}$$

For a given closed-loop system with an arbitrary linear control law, the stationary response is Gaussian-distributed, and consequently Eq. (61) can be restated as

$$R_{swj}\hat{\mathbf{e}}_j^{\mathrm{T}}\mathbf{\Phi}_{\mathbf{i}}\hat{\mathbf{e}}_j = V_{sw}\sqrt{\frac{2}{\pi}}[\hat{\mathbf{e}}_j^{\mathrm{T}}\mathbf{\Phi}_{\mathbf{i}}\hat{\mathbf{e}}_j]^{1/2}, \tag{63}$$

where $\mathbf{\Phi}_{\mathbf{i}} = \mathscr{E}[\mathbf{i}\mathbf{i}^{\mathrm{T}}]$, and where we have used the relation $\mathscr{E}[\,|g|\,] = \sigma\sqrt{2/\pi}$, for a random variable $g \sim N(0, \sigma)$. Thus,

$$\mathbf{R}_{sw}(\mathbf{\Phi}_{\mathbf{i}}) = V_{sw}\sqrt{\frac{2}{\pi}}\sum_{j=1}^{n_p}\hat{\mathbf{e}}_j[\hat{\mathbf{e}}_j^{\mathrm{T}}\mathbf{\Phi}_{\mathbf{i}}\hat{\mathbf{e}}_j]^{-1/2}\hat{\mathbf{e}}_j^{\mathrm{T}}. \tag{64}$$

In terms of $\mathbf{R}_{sw}(\mathbf{\Phi}_{\mathbf{i}})$, we can now state extensions to Theorems 1 and 2 for optimal control in the presence of semiconductor drive losses.

Theorem 3. *Let* $V_{sw} > 0$ *and* $\mathbf{R} \geqslant 0$. *Then the following statements generalize Theorems* 1 *and* 2, *respectively*:

(1) *Let* $\mathbf{F}$, $\mathbf{\Phi}_{\mathbf{i}}$, $\mathbf{\Phi}$, *and* $\mathbf{P}$ *be solutions to the following four simultaneous equations*:

$$\mathbf{0} = -\tfrac{1}{2}[\mathbf{A} + \mathbf{A}^{\mathrm{T}}] + \mathbf{A}^{\mathrm{T}}\mathbf{P} + \mathbf{P}\mathbf{A} - \mathbf{P}\mathbf{B}_{\mathbf{i}}[\mathbf{R} + \tfrac{1}{2}\mathbf{R}_{sw}(\mathbf{\Phi}_{\mathbf{i}})]^{-1}\mathbf{B}_{\mathbf{i}}^{\mathrm{T}}\mathbf{P}, \tag{65}$$

$$\mathbf{F} = -[\mathbf{R} + \tfrac{1}{2}\mathbf{R}_{sw}(\mathbf{\Phi}_{\mathbf{i}})]^{-1}\mathbf{B}_{\mathbf{i}}^{\mathrm{T}}\mathbf{P}, \tag{66}$$

$$\mathbf{0} = [\mathbf{A} + \mathbf{B}_{\mathbf{i}}\mathbf{F}]\mathbf{\Phi} + \mathbf{\Phi}[\mathbf{A} + \mathbf{B}_{\mathbf{i}}\mathbf{F}]^{\mathrm{T}} + \mathbf{B}_a\Phi_a\mathbf{B}_a^{\mathrm{T}}, \tag{67}$$

$$\mathbf{\Phi}_{\mathbf{i}} = \mathbf{F}\mathbf{\Phi}\mathbf{F}^{\mathrm{T}}, \tag{68}$$

where $\mathbf{R}_{sw}(\mathbf{\Phi_i})$ *is as in Eq.* (64). *Then* $\mathbf{F}:\mathbf{x}\to\mathbf{i}$ *is the linear state feedback controller optimizing* $\bar{P}_S$, *the corresponding value of which is*

$$\bar{P}_S = \Phi_a \mathbf{B}_a^{\mathrm{T}}[\tfrac{1}{2}\mathbf{I} - \mathbf{P}_{sw}]\mathbf{B}_a - \tfrac{1}{2}\mathrm{tr}[\mathbf{R}_{sw}(\mathbf{\Phi_i})\mathbf{\Phi_i}]. \tag{69}$$

(2) *Let* $\mathbf{L}$ *and* $\mathbf{W}$ *be solutions to Eqs.* (53) *and* (54). *Let* $\mathbf{F}$, $\mathbf{\Phi_i}$ *and* $\mathbf{P}$ *satisfy Eqs.* (65), (66), (68), *but with* $\mathbf{\Phi}\leftarrow\hat{\mathbf{\Phi}}$, *where* $\hat{\mathbf{\Phi}}$ *obeys*

$$\mathbf{0} = [\mathbf{A}+\mathbf{B_i F}]\hat{\mathbf{\Phi}} + \hat{\mathbf{\Phi}}[\mathbf{A}+\mathbf{B_i F}]^{\mathrm{T}} + \mathbf{L}\mathbf{\Phi}_n\mathbf{L}^{\mathrm{T}}. \tag{70}$$

Then $\mathbf{K}(s):\mathbf{v}\to\mathbf{i}$ *in Eq.* (52), *but with the new solution for* $\mathbf{F}$, *is the linear voltage feedback controller optimizing* $\bar{P}_S$, *the corresponding value of which is*

$$\bar{P}_S = \Phi_a \mathbf{B}_a^{\mathrm{T}}[\tfrac{1}{2}\mathbf{I} - \mathbf{P}]\mathbf{B}_a - \mathrm{tr}[\mathbf{W}\mathbf{F}^{\mathrm{T}}(\mathbf{R}+\mathbf{R}_{sw}(\mathbf{\Phi_i}))\mathbf{F}] - \tfrac{1}{2}\mathrm{tr}[\mathbf{R}_{sw}(\mathbf{\Phi_i})\mathbf{\Phi_i}]. \tag{71}$$

Proof. (1) Recall that the maximization of $\bar{P}_S$ is equivalent to the minimization of $\mathscr{E}[P_{\mathrm{diss}}]$. For any state feedback gain $\mathbf{F}$, $\mathscr{E}[\mathbf{x}\mathbf{x}^{\mathrm{T}}]=\mathbf{\Phi}$ is found through Lyapunov equation (67), and $\mathscr{E}[\mathbf{i}\mathbf{i}^{\mathrm{T}}]=\mathbf{\Phi_i}$ through Eq. (68). Then we have

$$\mathscr{E}[P_{\mathrm{diss}}] = \mathrm{tr}[(-\tfrac{1}{2}[\mathbf{A}+\mathbf{A}^{\mathrm{T}}] + \mathbf{F}^{\mathrm{T}}(\mathbf{R}+\mathbf{R}_{sw}(\mathbf{\Phi})_{\mathbf{i}})\mathbf{F})\mathbf{\Phi}]. \tag{72}$$

Optimality implies that

$$\frac{\partial}{\partial F_{ij}}\mathscr{E}[P_{\mathrm{diss}}] = \mathbf{0} \quad \forall i,j. \tag{73}$$

For the case without semiconductor losses (i.e., with $\mathbf{R}_{sw}(\mathbf{\Phi_i})=\mathbf{0}$), evaluation of this optimality condition leads directly to Eqs. (39) and (40). It is a standard linear algebra exercise to show that

$$\frac{\partial}{\partial F_{ij}}\mathrm{tr}[\mathbf{F}^{\mathrm{T}}\mathbf{R}\mathbf{F}\mathbf{\Phi}] = 2\{\mathbf{R}\mathbf{F}\mathbf{\Phi}\}_{ij} + \mathrm{tr}\left[\mathbf{F}^{\mathrm{T}}\mathbf{R}\mathbf{F}\frac{\partial}{\partial F_{ij}}\mathbf{\Phi}\right], \tag{74}$$

$$\frac{\partial}{\partial F_{ij}}\mathrm{tr}[\mathbf{F}^{\mathrm{T}}\mathbf{R}_{sw}(\mathbf{\Phi_i})\mathbf{F}\mathbf{\Phi}] = \{\mathbf{R}_{sw}(\mathbf{\Phi_i})\mathbf{F}\mathbf{\Phi}\}_{ij} + \frac{1}{2}\,\mathrm{tr}\left[\mathbf{F}^{\mathrm{T}}\mathbf{R}_{sw}(\mathbf{\Phi_i})\mathbf{F}\frac{\partial}{\partial F_{ij}}\mathbf{\Phi}\right]. \tag{75}$$

As such, switch resistance $\mathbf{R}_{sw}(\mathbf{\Phi_i})$ participates in optimality condition (73) in the same manner as if it were a linear resistance, but multiplied by a factor of $\frac{1}{2}$. Consequently, in the equations for optimal $\mathbf{F}$, analogous to Eqs. (39) and (40), this factor of $\frac{1}{2}$ appears, giving Eqs. (65) and (66). Using the solution to Eq. (65), we have that

$$\mathrm{tr}[(-\tfrac{1}{2}[\mathbf{A}+\mathbf{A}^{\mathrm{T}}] + \mathbf{F}^{\mathrm{T}}(\mathbf{R}+\tfrac{1}{2}\mathbf{R}_{sw}(\mathbf{\Phi})_{\mathbf{i}})\mathbf{F})\mathbf{\Phi}] = \Phi_a\mathbf{B}_a^{\mathrm{T}}\mathbf{P}\mathbf{B}_a. \tag{76}$$

This equation and (72) give Eq. (69) for the optimal $\bar{P}_S$.

(2) For the voltage feedback case, the existence of semiconductor dissipation has no impact on the optimal observer for the system, which is still the Kalman filter

$$\dot{\hat{\mathbf{x}}} = \mathbf{A}\hat{\mathbf{x}} + \mathbf{B_i i} + \mathbf{L}(\mathbf{v} - \mathbf{B}_{\mathbf{i}}^{\mathrm{T}}\hat{\mathbf{x}}), \tag{77}$$

with gain $\mathbf{L}$ defined as in Eqs. (53) and (54). The state covariance matrix $\mathbf{\Phi}$ is the summation of $\hat{\mathbf{\Phi}}=\mathscr{E}[\hat{\mathbf{x}}\hat{\mathbf{x}}^{\mathrm{T}}]$ and $\mathbf{W}=\mathscr{E}[(\mathbf{x}-\hat{\mathbf{x}})(\mathbf{x}-\hat{\mathbf{x}})^{\mathrm{T}}]$ where $\hat{\mathbf{\Phi}}$ is found through Eq. (70) and $\mathbf{W}$ through Eq. (54). Substitution into Eq. (72) results in a decoupling of $\mathbf{W}$, i.e., the problem is certainty-equivalent. For any feedback matrix $\mathbf{F}:\hat{\mathbf{x}}\to\mathbf{i}$, $\mathbf{\Phi_i}$ is again found through Eq. (68). Optimality of $\mathbf{F}$ is still defined by Eq. (73), and the remainder of the proof follows from Theorem 2 in an entirely analogous fashion to the way that proof (1) follows from Theorem 1. □

Both in the state and voltage feedback cases, the solution to the optimal controller involves the solution to five simultaneous equations, some of which are nonlinear. In general, these solutions do not have a closed form. However, note that for fixed $\mathbf{R}_{sw}$, these equations can be solved sequentially; first by finding $\mathbf{P}$, then $\mathbf{F}$, then $\mathbf{\Phi}$ (or $\hat{\mathbf{\Phi}}$ for output feedback), and finally $\mathbf{\Phi_i}$.

This observation gives rise to an iterative procedure for solving for the optimal linear feedback in the presence of switching losses, which applies equally to state and voltage feedback cases. We start from an initial guess for $\mathbf{R}_{sw}$, denoted $\mathbf{R}_{sw}^{(0)}$. Then, iteration k consists of:

(1) Given $\mathbf{R}_{sw}^{(k)}$, solve for the optimal $\mathbf{F}^{(k)}$.
(2) Find the resultant covariance matrix $\mathbf{\Phi}^{(k)}$ (or $\hat{\mathbf{\Phi}}^{(k)}$) for the closed-loop linear system, and the current covariance matrix as $\mathbf{\Phi}_{\mathbf{i}}^{(k)}$.
(3) Using $\mathbf{\Phi}_{\mathbf{i}}^{(k)}$, resolve for $\mathbf{R}_{sw}^{(k+1)}$ from Eq. (64) and go back to step 1 with $k \leftarrow k+1$.

No guarantees are made here regarding the uniqueness of convergence for this ad hoc routine. However, it is straightforward to prove that the algorithm does always converge, and produces monotonically increasing $\bar{P}_S$ for each successive $\mathbf{F}^{(k)}$. For the examples presented in this paper the routine did appear to converge to the same solution for arbitrary initial $\mathbf{R}_{sw}^{(0)}$.

4.1. Full-state feedback control

Consider the state-feedback control case, where $R_j = 0.1\,\Omega$ and $V_{sw} = 1.4\,\mathrm{V}$. Then the optimal controller, as well as the optimum efficiency, depends on the excitation intensity Φ_a. This is shown in Fig. 6, for which $\mathbf{F}$ was optimized as described above *for each* Φ_a. Two patch distributions are shown in the figure; one with $\{\ell_1, \ell_2\} = \{0.1\ell, 0.2\ell\}$ and the other with a single patch spanning the beam length. Also shown are the effective switch resistances, R_{swj}, as a function of Φ_a, for the optimized closed-loop system.

This plot has several key features. First, note that for Φ_a below the critical value (0.002 for the three-patch beam and 0.01 for the one-patch case) the energy harvesting becomes infeasible. This is because below this excitation level, the drive cannot be operated at all without dissipating more energy than is being transduced. Thus, below this excitation level, the "optimal control" is to do nothing. For values of Φ_a above this critical value, the efficiency of conversion rises, as the switch resistances decrease. Two benchmark lines are shown on the plot, signifying the optimal efficiency with $V_{sw} = 0$. The efficiencies in the presence of switching losses asymptotically approach this upper bound as $\Phi_a \to \infty$.

In the presence of semiconductor dissipation, plots analogous to Fig. 3 can be made to ascertain the sensitivity of η_{opt} to the patch lengths. This is shown in Fig. 7, for Φ_a values of 0.002, 0.01, 0.1, 1, 10, and

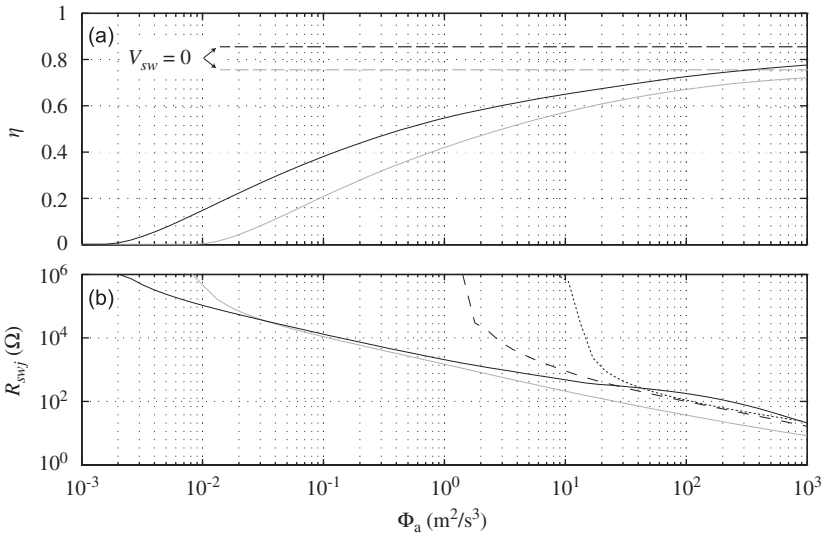

Fig. 6. Optimal efficiency (a) and switch resistances (b) for linear full-state control vs. Φ_a, for $\{\ell_1, \ell_2\} = \{0.1\ell, 0.2\ell\}$ (black) and the single-patch case (gray). Switch resistances in (b) are R_{sw1}, R_{sw2}, R_{sw3}.

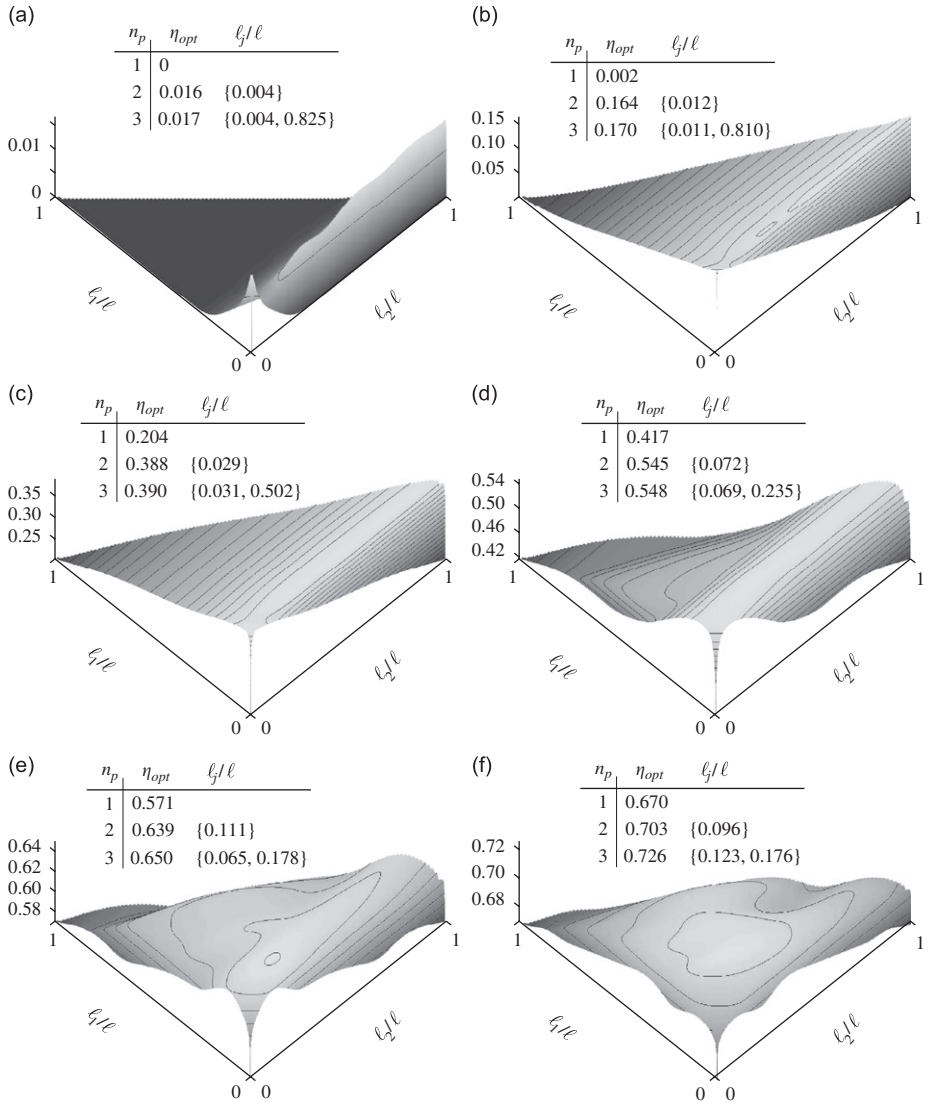

Fig. 7. Dependence of η_{opt} on $\{\ell_1, \ell_2\}$, with $\ell_3 = \ell - \ell_1 - \ell_2$, for $\Phi_a = 0.002$ (a), 0.01 (b), 0.1 (c), 1 (d), 10 (e), and $100\,\text{m}^2/\text{s}^3$ (f).

$100\,\text{m}^2/\text{s}^3$. Qualitatively, these plots give intuitive results, in the sense that as Φ_a becomes small, $\mathbf{R}_{sw}$ becomes large, resulting in lower optimal efficiencies. However, note that while the marginal increase between one and two patches is rather large in all cases, the marginal improvement from two to three patches only becomes significant for large Φ_a. We also note that for low Φ_a, the optimal efficiency corresponds to very small patch lengths, which are impractical. In this case, near-optimality can be obtained by using two patches, with the patch nearest to the root of the beam designed to be as short as possible.

4.2. Voltage feedback control

In the voltage feedback case, the design of $\mathbf{K}(s)$ follows in essentially the same manner as the full-state feedback case, and results similar to Fig. 6 follow. Assuming $\mathbf{\Phi}_n = \Phi_n \mathbf{I}$, we can investigate the way in which Φ_a and Φ_n influence the conversion efficiency η achieved by this design approach. Fig. 8 shows a contour plot η for the optimized $\mathbf{K}(s)$, as a function of Φ_a and Φ_n, and where we have used $\{\ell_1, \ell_2\} = \{0.1\ell, 0.2\ell\}$. As expected, the efficiency for any ratio Φ_n/Φ_a increases with Φ_a.

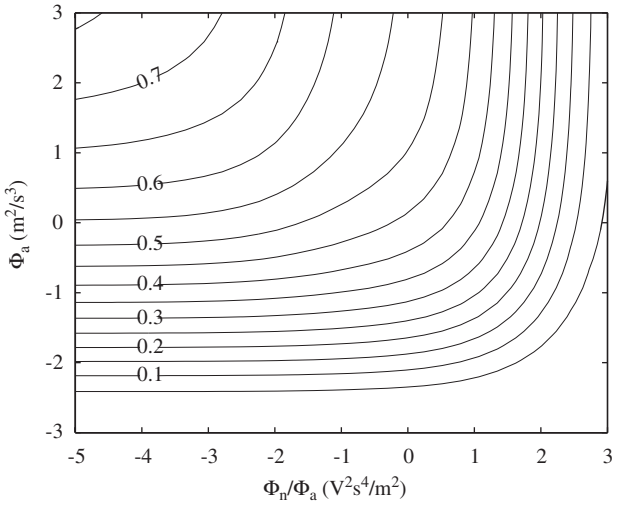

Fig. 8. Efficiency for optimal linear voltage feedback, vs. Φ_a and Φ_n, for $V_{sw} = 1.4\,\mathrm{V}$ and $R_j = 0.1\,\Omega$.

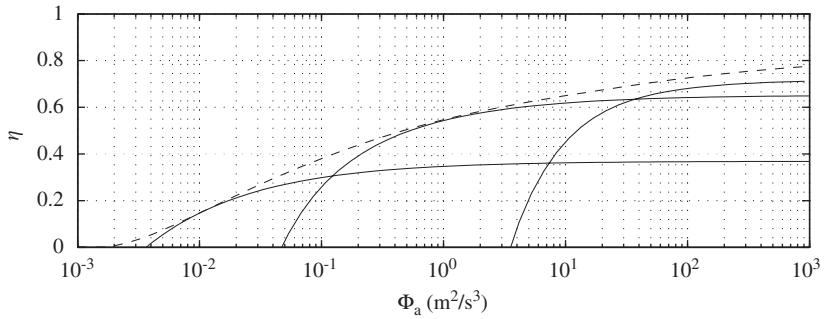

Fig. 9. Efficiency for linear output feedback controllers optimized for Φ_a values of 0.01, 1, and $100\,\mathrm{m^2/s^3}$.

4.3. Sub-optimal control

Results from this section have illustrated that both for state and voltage feedback, the optimal energy harvesting controller depends on excitation intensity Φ_a. In many applications, this may present a difficulty, because there may be significant uncertainty in Φ_a, or else it may vary over time. One solution to this would be to make the feedback controller adaptive to these different conditions. However, the computational resources associated with such an adaptive controller may require significant power, and this demand may exceed the power actually being generated. Consequently, a simpler linear time-invariant (yet sub-optimal) controller may be more appropriate.

Fig. 9 shows the sub-optimal conversion efficiencies for three linear voltage feedback controllers $\mathbf{K}(s)$, designed assuming Φ_a values of 0.01, 1, and $100\,\mathrm{m^2/s^3}$. For each design, a Φ_n value was assumed which resulted in a crossover frequency of approximately 1 kHz. For the three designs, this resulted in Φ_n values of 10^{-7}, 10^{-4}, and $10^{-1}\,\mathrm{V^2\,s}$. The plots in Fig 9 assume that this measurement noise is actually present in the system. If perfect measurements are alternatively assumed, the efficiencies increase slightly. For reference, the optimal efficiency with full-state feedback (i.e., from Fig 6) is also shown. As can be seen, there is definitely a price to be paid for sub-optimal control design, as all three controllers exhibit performance well below the maximum physically attainable performance, for Φ_a away from the design value. In the case of the controller optimized for $\Phi_a = 100\,\mathrm{m^2/s^3}$, the performance of the controller is further hampered by the restriction on bandwidth, which accounts for why its efficiency falls well short of reaching that of optimal state feedback, even at the design point at $\Phi_a = 100\,\mathrm{m^2/s^3}$.

5. Conclusions

This paper has presented a systematic approach to the design of control systems for energy harvesting applications. Although the focus has been on harvesting energy from piezoelectric bimorph beams, the theory is applicable more broadly. It is appropriate in circumstances where the external input can be justifiably modeled as a broadband acceleration, and is applicable to arbitrarily large networks of coupled transducers, and to systems with many resonant modes. The main conclusions of this analysis can be summarized as follows:

(1) In the presence of resistive drive impedances, the optimal control of energy harvesting systems for maximal power generation is a linear state feedback law, which can be derived using standard state feedback $\mathscr{H}_2$ control theory. The case of a lossless drive model can be interpreted as a "cheap control" problem, although the optimal control gain becomes infinitely large as the drive resistance approaches zero.
(2) In the presence of resistive drive impedances and broadband measurement noise, the optimal transducer voltage feedback law is a linear dynamic controller, and its design can be framed as a standard output-feedback $\mathscr{H}_2$ control problem. In this case, the optimal controller as well as the optimal power conversion efficiency depends on the sound-to-noise ratio Φ_a/Φ_n.
(3) The closed-form nature of these optimal control designs makes it straightforward to concurrently optimize hardware and control for maximal conversion efficiency.
(4) These control design techniques can be extended to systems with combined resistive and semiconductor drive dissipation, using an iterative design approach. The resultant optimal control policy, and the optimal conversion efficiency, will in general depend on the level of external excitation as well as the measurement noise.

This analysis raises many questions. For example, in many applications the measurement noise associated with transducer voltage feedback may not be the dominant hurdle the system must overcome to achieve maximal efficiency. Rather, bandwidth restrictions, or controller order limitations, may be the primary limiting factors in the design. Additionally, this analysis does not take into account some power demands, such as that required to operate the control intelligence and gate the mosfets in the drive circuitry. Although these issues may be more difficult to treat directly in a theoretical context, this may be necessary in order to get the clearest picture of the constraints impinging on control and hardware design.

References

[1] S.R. Anton, H.A. Sodano, A review of power harvesting using piezoelectric materials (2003–2006), *Smart Materials & Structures* 16 (2007) R1–R21.
[2] G.K. Ottman, H.F. Hofmann, A.C. Bhatt, G.A. Lesieutre, Adaptive piezoelectric energy harvesting circuit for wireless remote power supply, *IEEE Transactions on Power Electronics* 17 (2002) 669–676.
[3] G.K. Ottman, H.F. Hofmann, G.A. Lesieutre, Optimized piezoelectric energy harvesting circuit using step-down converter in discontinuous conduction mode, *IEEE Transactions on Power Electronics* 18 (2003) 696–703.
[4] G.A. Lesieutre, G.K. Ottman, H.F. Hofmann, Damping as a result of piezoelectric energy harvesting, *Journal of Sound and Vibration* 269 (2004) 991–1001.
[5] A. Kasyap, J. Lim, D. Johnson, S. Horowitz, T. Nishida, K. Ngo, M. Sheplak, L. Cattafesta, Energy reclamation from a vibrating piezoceramic composite beam, *Proceedings of the Ninth International Congress on Sound and Vibration*, Orlando, FL, July 8–11, 2002.
[6] Y.C. Shu, I.C. Lien, Analysis of power output for piezoelectric energy harvesting systems, *Smart Materials & Structures* 15 (2006) 1499–1512.
[7] Y.C. Shu, I.C. Lien, Efficiency of energy conversion for a piezoelectric power harvesting system, *Journal of Micromechanics and Microengineering* 16 (2006) 2429–2438.
[8] S. Roundy, P. Wright, J. Rabaey, A study of low level vibrations as a power source for wireless sensor nodes, *Computer Communications* 26 (2003) 1131–1144.
[9] A. Badel, D. Guyomar, E. Lefeuvre, C. Richard, Piezoelectric energy harvesting using a synchronized switch technique, *Journal of Intelligent Material Systems and Structures* 17 (2006) 831–839.
[10] D. Guyomar, C. Magnet, E. Lefeuvre, C. Richard, Nonlinear processing of the output voltage of a piezoelectric transformer, *IEEE Transactions on Ultrasonics Ferroelectrics and Frequency Control* 53 (2006) 1362–1375.

[11] D. Guyomar, C. Magnet, E. Lefeuvre, C. Richard, Power capability enhancement of a piezoelectric transformer, *Smart Materials & Structures* 15 (2006) 571–580.
[12] K. Makihara, J. Onoda, T. Miyakawa, Low energy dissipation electric circuit for energy harvesting, *Smart Materials & Structures* 15 (2006) 1493–1498.
[13] J. Rastegar, C. Pereira, H.L. Nguyen, Piezoelectric-based power sources for harvesting energy from platforms with low frequency vibration, *Proceedings of SPIE Smart Structures and Materials Conference*, San Diego, CA, February 26–March 2, 2006.
[14] S.M. Shahruz, Design of mechanical bandpass filters for energy scavenging, *Journal of Sound and Vibration* 292 (2006) 987–998.
[15] N. Hagood, W. Chong, A. von Flotow, Modelling of piezoelectric actuator dynamics for active structural control, *Journal of Intelligent Materials Systems and Structures* 1 (1990) 327–354.
[16] H. Sodano, G. Park, D. Inman, Estimation of electric charge output for piezoelectric energy harvesting, *Strain* 40 (2004) 49–58.
[17] J.T. Scruggs, Multi-objective optimal control of vibratory energy harvesting systems, *Proceedings, SPIE 15th Annual International Symposium on Smart Structures and Materials*, San Diego, CA, March 9–13, 2008.
[18] J. Kassakian, M. Schlecht, G. Verghese, *Principles of Power Electronics*, Addison-Wesley, Reading, MA, 1991.
[19] J. Main, D. Newton, L. Massengill, E. Garcia, Efficient power amplifiers for piezoelectric applications, *Smart Materials & Structures* 6 (1996) 766–775.
[20] S. Chandrasekaran, D. Lindner, R. Smith, Optimized design of switching amplifiers for piezoelectric actuators, *Journal of Intelligent Materials Systems and Structures* 11 (2000) 887–901.
[21] K.J. Astrom, *Introduction to Stochastic Control Theory*, Academic Press, New York, 1970.
[22] R. Clough, J. Penzien, *Dynamics of Structures*, McGraw-Hill, New York, 1975.
[23] B. Anderson, J. Moore, *Optimal Control: Linear Quadratic Methods*, Prentice-Hall, Englewood Cliffs, NJ, 1990.
[24] H. Kwakernaak, R. Sivan, The maximally achievable accuracy of linear optimal regulators and linear optimal filters, *IEEE Transactions on Automatic Control* 17 (1972) 79–85.
[25] A. Jameson, R.E. O'Malley, Cheap control of the time-invariant regulator, *Applied Mathematics and Optimization* 1 (1975) 337–354.
[26] C. Scherer, P. Gahinet, M. Chilali, Multiobjective output-feedback control via LMI optimization, *IEEE Transactions on Automatic Control* 42 (1997) 896–911.